LBNL-42778
Preprint

ERNEST ORLANDO LAWRENCE
BERKELEY NATIONAL LABORATORY

Femtosecond Studies of Electron Dynamics at Surfaces

Nien-Hui Ge, Chung M. Wong,
and Charles B. Harris

Chemical Sciences Division

November 1998

Submitted to
Accounts of
Chemical Research

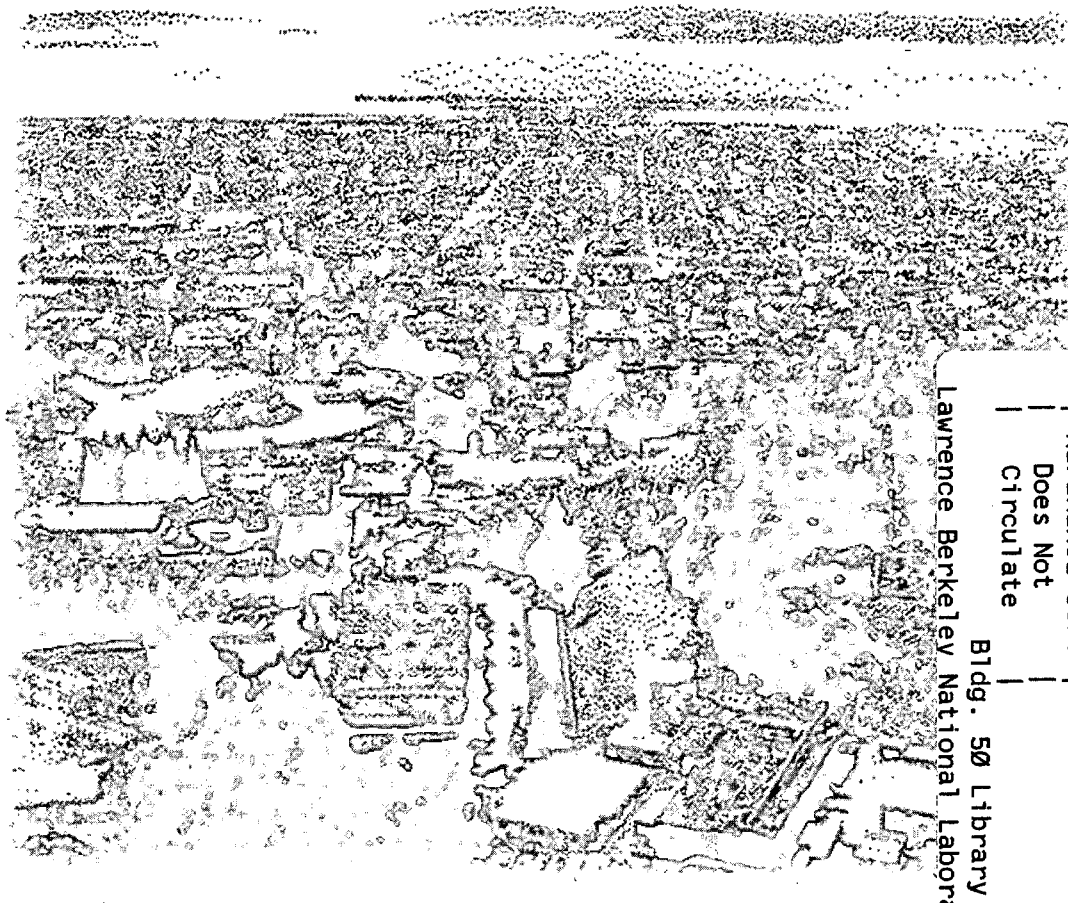

DISCLAIMER

Femtosecond Studies of Electron Dynamics at Surfaces

Nien-Hui Ge, Chung M. Wong, and Charles B. Harris*

Department of Chemistry, University of California, Berkeley, California, 94720

and

Chemical Sciences Division, Ernest Orlando Lawrence Berkeley National Laboratory, Berkeley, California, 94720

Introduction

The study of electron behavior at interfaces between dissimilar materials constitutes a major research area at the present time. For example, recent progress in organic light-emitting devices[1] has heightened the demand for a deeper understanding of electronic processes at metal-organic interfaces, let alone other technologically important devices. Electron trapping, scattering, and the potential barrier at the interface can drastically affect carrier transport properties and the performance of devices. In order to develop a microscopic understanding of the behavior of electrons in complex media, a systematic study of the energy levels and dynamics of electrons associated with model interfaces is required.

The development of ultrahigh-vacuum technology and surface preparation methods over the past 30 years has enabled researchers to grow ultrathin atomic and molecular adlayers on single crystal substrates. This offers an opportunity to investigate properties associated with Ångstrom-scale materials in a well-controlled fashion. To fully explore excited state dynamics of electrons at interfaces, experimental techniques must provide band-structure specificity, as well as time resolution. The conventional means of determining the band structure of excited surface electronic states is angle-resolved inverse photoemission spectroscopy.[2] This technique has been very successful, but has limited energy resolution and cannot be

*To whom correspondence should be addressed.

time-resolved. Scanning tunneling spectroscopy[3] provides information on unoccupied energy levels with atomic resolution, but also has limited energy resolution and only under ideal situations provides time resolution. Femtosecond two-photon photoemission (TPPE)[4,5] has an order of magnitude better energy resolution than either of these techniques and the ability to achieve time resolution of 30 femtoseconds.[6] Femtosecond TPPE combined with angle-resolution provides a powerful tool in resolving electron momentum relaxation and the process of electron localization in real time.

Several review articles have been published regarding electron dynamics at surfaces, including semiconductor and metal surfaces as well as surfaces covered with adsorbates and metallic overlayers.[5,7–10] In this Account we will focus on the study of ultrafast electron dynamics at metal-dielectric interfaces. Our goal is to answer fundamental questions such as the following: First, how do the dielectric properties and electronic structure of the overlayer affect the electron dynamics and the interfacial potential that electrons experience? Second, how does the electron coupling to the metal substrate change as the dielectric layer increases in width in a layer-by-layer fashion? Lastly, electrons in metals are usually free-electron–like, but electrons in dielectric solids are usually localized. How does the transition of the electronic behavior occur at the interface and what do we expect the spatial extent of interfacial electrons to be? In the following sections, we present results and discuss in detail the electronic tunneling processes and self-trapping of image electrons at alkane/Ag(111) interfaces.

Background

Femtosecond Angle-Resolved Two-Photon Photoemission. The two photons in TPPE correspond to a pump pulse which excites electrons from occupied states to unoccupied intermediate states and a probe pulse which ejects the excited electrons (Fig. 1A). The difference between the measured electron kinetic energy, E_{kin}, and the probe photon energy yields the binding energy of the intermediate state. The decay of the photoelectron signal

with increasing time delay between the pump and the probe pulse is a direct measurement of the lifetime.

The band structure of the intermediate state can be mapped out by measuring the angle dependence of the photoelectron kinetic energy (Fig. 1B). Because photoemission at well-ordered interfaces preserves parallel momentum ($\hbar k_{||}$),[11] $k_{||}$ can be obtained by $k_{||} = (2m_e E_{kin}/\hbar^2)^{1/2} \sin\theta$, where m_e is the free electron mass and θ is the emission angles. For electrons that are delocalized parallel to the interface, the angle-resolved TPPE data will exhibit a dispersive band. The energy of these electrons is given by

$$E = E_0 + E_{||} = E_0 + \hbar^2 k_{||}^2 / 2m^*, \tag{1}$$

where E_0 is the onset of the interfacial band at $k_{||} = 0$, and m^* the electron effective mass. The deviation of m^* from m_e is a measure of the coupling of the electron with the bulk or an overlayer. Spatially localized electrons, on the other hand, result in non-dispersive features in the spectra as a function of the emission angle.

Image States on Bare Metal Surfaces. An electron outside a conducting metal surface interacts with the polarization it induces at the surface (Fig. 2). This interaction gives rise to a 1–D Coulomb potential, $-1/4z$, which supports a Rydberg series of image states[12] converging towards the vacuum level (Fig. 2) with binding energies $E_n \approx -0.85\ \mathrm{eV}/n^2$, where $n = 1, 2 \ldots$ is the quantum number.

The lifetime of the image electrons depends mainly on the electron's ability to couple to the substrate empty band structure. Theoretically, the lifetime is predicted to vary as n^3 since the electron density moves away from the metal surface with increasing n (Fig. 2) which decreases its spatial overlap with the metal bulk.[12] This prediction has been experimentally confirmed.[13,14]

While the image states are localized perpendicular to the surface, parallel to the surface the electrons are delocalized (Fig. 1B, Eqn. 1 with $E_0 = E_n$). On many metal surfaces $m^* \approx m_e$ were found.[5]

Electron Tunneling at Metal-Alkane Interfaces

We will now consider the effect of n-alkane overlayers on image states. Low energy electron diffraction studies have shown that n-alkanes grow ordered layers on the Ag(111) surface with the carbon-carbon bonds parallel to the surface.[15] Figure 3 shows the TPPE binding energy spectra at 0° emission upon the adsorption of n-heptane. The image state series persist and become less bound with increasing coverage.[8] This change in binding energy clearly corresponds to a layer-by-layer evolution of the surface potential.

Even more dramatic changes are seen in the electron lifetimes. Table 1 summarizes the lifetime data extracted from the time-resolved measurements.[6] First, the n-dependence of the image state lifetime for the bare surface is very different from that of the monolayer covered surface. For the bare surface, the $n = 2$ lifetime is actually shorter than $n = 1$, in contrast to the simple n^3 expectation. It has been attributed to the fact that on Ag(111) the $n = 1$ state is located within the projected bulk band gap, while the $n \geq 2$ image states are located outside the band gap (Fig. 2) and get substantially broadened due to the direct coupling to energetically degenerated bulk band states.[13,16] The adsorption of the monolayer, however, not only dramatically increases the image state lifetimes but also allows the lifetime to assume the monotonic dependence on n. According to the previous measurements of the Ag(111) band gap[5] and our measurements of the work function shift upon n-heptane adsorption, $n = 2$ moves into the gap in the presence of a monolayer but $n = 3$ is still degenerate with the bulk conduction band. Therefore, the mere change in degeneracy can not explain this behavior. Rather, the significant modification of the surface potential by the layer may be the primary cause. Solid and liquid alkanes generally possess a bulk electron affinity repulsive by a few tenths of an electron volt.[17] This repulsive interaction may serve to weaken the coupling of the electron to the bulk states, even for a monolayer. Similar arguments has been applied to compare the $n = 3$ lifetimes of cyclohexane and Xe monolayers.[18]

Secondly, examining the $n = 1$ lifetime as the coverage increases from monolayer to

trilayer, the approximately exponential increase in lifetime indicates that increasing the adlayer thickness presents the image electron with a wider barrier through which it must tunnel in order to decay back into the metal. The existence of the tunneling barrier is consistent with the repulsive electron affinity of the longer chain n-alkanes in the condensed phase.

Thirdly, the increase of the $n = 2$, 3 lifetimes with coverage is less dramatic than $n = 1$. This indicates that the $n = 2$ and 3 states are less influenced by the increasing width of the tunneling barrier because they are 500 to 600 meV higher in energy than the $n = 1$ state. This difference in the effect of the tunneling barrier for the various quantum levels is clearly seen in the bilayer and trilayer columns of Table 1. The lifetime is no longer a monotonic function of n, with the $n = 1$ lifetime being the longest. The essential physics of the preceding paragraphs is illustrated below by comparing our data to the results of model calculations.

Dielectric Continuum Model.[19] In the vacuum region, the electrostatic energy of a point charge outside a metal covered with a continuum dielectric overlayer of thickness d and dielectric constant ϵ is given by[19]

$$V(z,d) = \frac{-\beta e^2}{4(z-d)} + \frac{(1-\beta^2)e^2}{4\beta}\sum_{j=1}^{\infty}\frac{(-\beta)^j}{z-d+jd}, \quad z > d, \tag{2}$$

where $\beta = (\epsilon - 1)/(\epsilon + 1)$. The first term is the attractive image potential induced by an excess electron outside an infinite dielectric. The second term describes the influence of the metal. Inside the dielectric, the potential can be taken as[19]

$$V(z) = -\frac{e^2}{4\epsilon z} + V_0, \tag{3}$$

where the first term is the metal image potential screened by the presence of the dielectric layer, and V_0 is the bulk electron affinity (conduction band minimum with respect to the vacuum level) of the dielectric. The appearance of V_0 as an additive constant to the potential provides the simplest description of the overlayer band structure.

Using parameters $\epsilon = 2.0$ and $V_0 = 0.2$ eV that are reasonably close to those of bulk n-octane, the potential for the bilayer case is shown in Fig. 4A. Solving the Schrödinger

equation gives $n = 1$ binding energies that are in good agreement with the experiment for up to ten layers of n-octane (Fig. 5).[6] From the calculated electron probablity density (Fig. 4B), we see that the electrons tend to be excluded from the layer due to the potential barrier set up by the repulsive electron affinity of the alkane layer. As the layer thickness increases, the coupling to the metal decreases and electrons become less bound.

We will now examine the effect of the tunneling barrier on image state lifetimes. On bare metal surfaces, the lifetime n^3 dependence can also be thought of as being due to the n^3 variation of the classical period of motion in the potential well, which constitutes an "attempt rate" for penetration into the bulk of the metal substrate. With the presence of electron repulsive overlayer, the probability of tunneling through the effective potential barrier determines how likely a decay attempt is successful (Fig. 4). The lifetime of the electrons is then determined by both the classical oscillation time in the vacuum image potential and the tunneling probability.[19] Adapting a model by Cole[19] in which the WKB approximation is used to calculate the tunneling probability and scaling the calculation by the bare surface lifetime,[6,20] we can correctly reproduce both the layer thickness and quantum number dependence of the lifetime (Table 1).

In contrast to the results of n-alkanes, systems like neopentane or Xe should exhibit very different behavior because these materials possess attractive bulk electron affinities which can provide an interfacial potential well that electrons tend to be drawn into. In fact, the TPPE studies of multilayer Xe/Ag(111)[18,21] indicates quantum confinement effects in the Xe slab. As the Xe layer thickness increases, the $n = 2, 3$ image states of the bare metal evolve into quantum well states of the layer and becomes more bound just like a particle in a box.[21] Concomittently, electron lifetime as a function of layer thickness displays a characteristic oscillation.[18] The drastically different results for n-alkane and Xe overlayers clearly shows that the dynamics of excess electrons are largely determined by the electron affinity of the adsorbates.

Electron Localization at Metal-Alkane Interfaces

We next examine the lateral motion of the electron in the presence of an alkane overlayer. In the previous static angle-resolved TPPE studies of various alkane/Ag(111) interfaces,[22] besides the parabolically dispersing feature normally expected for the delocalized $n = 1$ image electrons, a nondispersive peak was observed and attributed to localized electronic states. These localized features were seen only for cyclohexane and various straight chain alkanes, but not for neopentane.[22] This observation was correlated with excess electron mobility in nonpolar liquids.[17] Localization was not seen for the $n = 2$ electron in the presence of monolayers and bilayers of some straight chain alkanes, presumably because the electron density is further away from the interface and thus the interaction with the adlayer is less.

In order to further elucidate the time scale of the localization process and the mechanism, a femtosecond time-resolved study is highly desirable. Angle-resolved TPPE spectra for bilayer n-heptane at 120 K with pump-probe delays of zero and 1670 fs are shown in Fig. 6.[23] These data clearly reveal that the delocalized state appears right after pump pulse excitation and there is a time delay in the formation of the localized state. Similar behavior is also found on a monolayer and a trilayer. Furthermore, the localized electrons exhibit no angle dependence in their 360-fs rise and 1600-fs decay dynamics (Fig. 7B), showing that all of the constituting $k_{||}$ plane wave components have the same dynamics, as expected for photoemission from a single state. In contrast, the rise and decay of the delocalized states have strong angle dependence (Fig. 7A).

The strong $k_{||}$-dependence of the delocalized state lifetime suggests that decay mechanisms other than direct decay back into the metal are operative. One possibility is intraband momentum relaxation to a different $k_{||}$ state and such relaxation may in turn result in an angle dependence of the rise time of the delocalized state. Our data show a much weaker $k_{||}$-dependence than the $k_{||}^4$-dependence of linewidth broadening predicted for the Auger process on bare metal surfaces.[12] We can therefore eliminate the contribution from this process

because the adlayer will weaken interaction between the image electrons and the bulk metal electrons.[24] Another possibility is the scattering of the image electrons with phonons of the alkane layers. However, a temperature dependence study on bilayer for a range of angles shows that delocalized states at 50 K decay faster than at 120 K, contradicting the phonon scattering theory prediction and indicating the need for other mechanisms. We note that the decay times of the delocalized states are of the same order as the rise time of the localized state. In fact, they correspond even at different temperatures. Both rates become faster as the temperature is lowered from 120 to 50 K. Such a temperature dependence of the $n = 1$ delocalized state is opposite to that of the bilayer $n = 2$ state[25,26] and bare $n = 1$ state[25] which are delocalized and do not show localization. These observations indicate that the delocalized electron primarily decays into the localized state and the localization time not only depends on its initial parallel momentum but also exhibits a non-Arrhenius temperature dependence.

In the search for a plausible localization mechanism, we can eliminate some of the possible candidates based on the following experimental observation. Firstly, extensive investigation of different layer preparation methods and annealing procedures found no difference in the relative intensity of the localized peak. Secondly, the proportion of monolayer patches interspersed with bilayer (apparent in Fig. 6B) can be varied by a factor of 5 without variation in the bilayer dynamics. These experiments shows that no amounts of defects or disorder in the layer that we could control had any significant effects on localization. Thirdly, the localized peak and the delocalized peak are very close in energy at $k_{||} = 0$ with a difference $\Delta E_0 \leq 10$ meV (Fig. 6). The fact that ΔE_0 is small suggests that impurity-enhanced localization is unlikely because one would expect a much larger ΔE_0 if localization were caused by electron trapping around impurities chemically distinct from n-alkane. Furthermore, it appears that the energy of the localized state is pinned to the bottom of the delocalized band regardless of layer composition (chain length) and thickness. The invariance of ΔE_0 versus layer thickness rules out localization due to confinement on small adsorbate islands[27] or vacancies. On a monolayer the depth of the potential well formed by vacancies of one-

monolayer thickness is higher than that on a bilayer. In order to make ΔE_0 invariant, the confinement energy shift on the former has to be higher by the same amount. One would not expect this to be a general case but at the mercy of a particular layer growth condition.

Small polaron formation. The most plausible mechanism for the above localization phenomena is the self-trapping of electrons in small polarons, originally conceived by Landau.[28] Electrons in rigid periodic lattices are delocalized, forming Bloch band states that are free-electron–like. In a deformable lattice, however, the electron-lattice interaction causes an electron to always carry with it a self-induced lattice deformation. The composite particle is called a polaron. "Small" polarons involve strong lattice distortion and the wavefunctions of the electrons are self-trapped to dimensions of a lattice spacing. Their motion between lattice sites can be described as a hopping process,[29] a behavior observed for charged carriers in many nonmetallic systems,[30,31] including molecular solids.[32]

Qualitatively, the degree of localization of carriers is determined by a balance of two competing tendencies (Fig. 8). *Delocalization* is favored by a lowering in kinetic energy equal to approximately half the band width, B. If an electron were localized in the lattice without inducing lattice distortion, that is, along the $Q = 0$ axis, its energy would increase to roughly the middle of the band because a spatially localized wavepacket contains all of the Bloch waves in the band due to the uncertainty principle. On the other hand, *localization* is encouraged by releasing the lattice relaxation energy, E_{rel}, when the electron is trapped at a single lattice site by the lattice polarization and distortion it causes. If the potential well is deep enough such that self-trapping energy $E_{\text{st}} \equiv E_{\text{rel}} - B$ is positive, the self-trapped state will be energetically favorable and a small polaron will form.

The balance between these opposing tendencies depends on the dimensionality of the lattice and the nature and the strength of its coupling with the electron. For a short-range electron-lattice coupling, which is the case for electrons in non-polar alkane solids, theoretical analysis has shown[33–35] that localization is energetically favored over delocalization in 1–D, and vice versa in 3–D. In a 2–D system, however, these two tendencies are nearly canceled. Thus two dimensionality is often called the marginal case.[35,36]

Our data are well explained by the above 2–D small polaron formation model. The lattice and the molecules that comprise it respond to the presence of an excess electron on the time scale of the lattice and molecular vibrational periods. This manifestates in the time delay between the population of the image state (Fig. 6A) and the formation of the localized self-trapped electrons (Fig. 6B). The small self-trapping energy, as measured by $\Delta E_0 \leq 10$ meV, indicates the existence of a delicate balance between the delocalizing and localizing tendencies in this system. This is consistent with a 2–D self-trapping picture based on the invariance of ΔE_0 versus layer thickness. Each additional alkane layer only modifies the interfacial potential normal to the interface, without affecting the trapping process parallel to the interface, leaving $E_{\rm st}$ unchanged. The self-trapped electron wavefunction can still be decomposed into a lateral component which is localized to dimensions comparable to the alkane unit surface mesh (Fig. 8), and a vertical component which is the usual 1–D image state wavefunction (Fig. 4B). The lifetime of the self-trapped electron is $k_{||}$-independent (Fig. 7B), but is dramatically lengthened with increasing alkane layer thickness as shown in Table 1. The data listed in the $n = 1$ row actually refer to the decay time of the localized state. The tunneling model in the previous section explains the decay mechanism of the localized state and suggests that the self-trapped electron is localized at the layer-vacuum junction (Fig. 4B) rather than at the layer-metal junction. The self-trapping process is associated with interactions between the electron and the topmost plane of the alkane molecules without rearrangement of the layer below.

Self-trapping dynamics. Furthermore, the small polaron model predicts a self-trapping time dependent on the electron's momentum. Inspecting the potential surfaces of the delocalized and self-trapped states (Fig. 8), one sees that an energetically favorable pathway to get from $V_{\rm f}$ to $V_{\rm s}$ without first reaching the point C involves thermal activation of the lattice to a configuration where the energy of the system is the same on both sides, *i.e.* the crossing point of $V_{\rm f}$ and $V_{\rm s}$. The energy difference between the crossing point and $V_f(k_{||})$ at $Q = 0$ represents the potential barrier or the activation energy for self-trapping. The self-trapping barrier is large at $k_{||} = 0$, decreases with $k_{||}$ until reaching the point C

where there is no barrier, then turns around to increase with $k_{||}$. Thus, the self-trapping rate is $k_{||}$-dependent. This description of the self-trapping process is analogous to the theory for electron transfer reactions[37,38] in the classical limit where the system has a thermal energy higher than the nuclear vibrational energy. A self-trapping process that starts from an initial state of particular $k_{||}$ with band energy $E_{||}$ and then proceeds to the self-trapped state corresponds to an electron transfer reaction with exothermicity of $-\Delta\mathcal{E} = E_{\rm st} + E_{||}$. Within the displaced harmonic potential approximation, the rate goes through the so-called Marcus inverted region when the exothermicity is equal to the reorganization energy, $-\Delta\mathcal{E} = E_{\rm rel}$.

We obtained the self-trapping rate by subtracting a $k_{||}$-independent tunneling rate (previous section) from the delocalized state decay rate. To obtain a good fit of its dependence on $-\Delta\mathcal{E}$ using the classical theory, however, requires an unreasonable adjustment of the temperature.[23] The observed non-Arrhenius temperature dependence also suggests the inadequacy of the classical theory. Electrons in a molecular lattice can interact with both intra- and intermolecular vibrations, forming molecular and lattice polarons, respectively.[32] In our temperature range, the low-frequency intermolecular vibrations can be treated classically, while the high-frequency intramolecular modes are frozen and require a quantum-mechanical treatment. We made the simplest assumption that self-trapping involves a single quantum-mechanical intramolecular mode with a frequency $\omega_{\rm q}$ and a reorganization energy $E_{\rm rq}$, and all other intermolecular modes are classical with a reorganization energy $E_{\rm rc}$. Without knowing the strength of the electronic coupling, $H_{\rm fs}$, between the delocalized and self-trapped states, it is hard to determine whether the process is adiabatic or non-adiabatic. Therefore, we analyzed the data in terms of a recently developed approach[39] in which the path integral technique is utilized to sum over all perturbation orders in electronic coupling. This formalism can work continuously from the non-adiabatic to the adiabatic regimes with its first order term coinciding exactly with the exact quantum mechanical expression for the nonadiabatic rate.

Figure 9A shows the result of our analysis.[23] The parameters $E_{\rm rc}$ and $E_{\rm rq}$ extracted from the fit are consistent with the interaction energies of lattice and molecular polarons

in organic molecular solids.[32] The energy of $\hbar\omega_q$ suggests that self-trapping involves the methylene rocking mode of n-heptane molecules.[40] Note that the first order term in the path integral accounts for nearly 96% of the fit in Fig. 9A. Therefore, the self-trapping process at 120 K can be well described by a non-adiabatic theory. However, the higher order terms become more important at lower temperatures. Figure 9B shows that the non-Arrhenius temperature dependence of the self-trapping rate at $-\Delta\mathcal{E} = 0.14$ eV is reproduced with no additional adjustment of parameters. The first order term accounts for only 83% of the rate for the data point at 50 K.

Further support of the small polaron formation picture comes from the wavelength dependence of the rise time of the localized state[25]. The rate at which the self-trapped electrons form is an averaged sum over self-trapping rates from all $k_{||}$ states. With 300 nm pump/600 nm probe, a wide range of $k_{||}$ (0–0.4 Å^{-1}) states can be populated, and they can all decay into the localized state, giving rise to a 360 fs rise (Fig. 7B). Selectively populating a narrower range of high $k_{||}$ states with fast self-trapping rate should reduce the rise time. This prediction is born out by the results obtained for 335 nm pump/670 nm probe by which only states with $k_{||} \sim 0.15$–0.17 Å^{-1} can be populated, resulting in a faster rise by a factor of ~ 2.

Conclusions

In this Account, we have discussed the application of time- and angle-resolved TPPE to the study of excess electron dynamics at metal-dielectric interfaces on the femtosecond time scale. First we monitored the layer-by-layer evolution of the interfacial electronic structure and dynamics. Such a study provides information on the nature of the interfacial potential. It is found that the electron affinity of the overlayer material strongly affects the dynamics and energies of the interfacial excited states. The formation of a tunneling barrier or potential well at the interface due to the presence of the adlayer plays a very important role in determining the spatial distribution of the interfacial electrons as well as the electronic

coupling across the interface.

We have also shown that an initially delocalized electron at the metal-alkane interface undergoes 2–D self-trapping within a few hundred femtoseconds. Our analysis shows that self-trapping involves inter- and intramolecular vibrational modes of the overlayer and the non-Arrhenius temperature dependence is a result of a strong quantum contribution from the intramolecular modes. These results for a model interface contribute to the fundamental understanding of electron behavior at the interface between metals and molecular solids. For example, similar localized states may exist at metal-polymer interfaces and contribute to their electronic properties. Time- and angle-resolved TPPE is a powerful and general probe that can provide detailed experimental information on electron dynamics at interfaces.

Acknowledgments

We gratefully acknowledge Dr. Robert L. Lingle, Jr., Jason D. McNeill, Robert E. Jordan, and Kelly J. Gaffney, who were involved in many of the experiments that are discussed and referenced in this paper. We particularly thank Prof. Xueyu Song for very helpful discussions. This work was supported by the Director, Office of Energy Research, Office of Basic Energy Sciences, Chemical Sciences Division of the U. S. Department of Energy, under Contract No. DE-AC03-76SF00098. The authors acknowledge NSF support for specialized equipment used in some experiments described herein.

REFERENCES

(1) Sheats, J. R.; Antoniadis, H.; Hueschen, M.; Leonard, W.; Miller, J.; Moon, R.; Roitman, D.; Stocking, A. Organic Electroluminescent Devices. *Science.* **1996**, *273*, 884–888.

(2) Himpsel, F. J. Inverse Photoemission from Semiconductors. *Surf. Sci. Rep.* **1990**, *12*, 1–48.

(3) Avouris, P. Probing the Wave Properties of Electrons and Manipulating Atoms at Surfaces with the Scanning Tunneling Microscope. *Account. Chem. Res.* **1994**, *27*, 159–165.

(4) Giesen, K.; Hage, F.; Himpsel, F. J.; Riess, H. J.; Steinmann, W. Two-Photon Photoemission via Image-Potential States. *Phys. Rev. Lett.* **1985**, *55*, 300–3.

(5) Fauster, T.; Steinmann, W. Two-Photon Photoemission Spectroscopy of Image States. In *Photonic Probes of Surfaces*; Halevi, P., Ed.; Elsevier: Amsterdam, 1995; pp. 347–411.

(6) Lingle, Jr., R. L.; Ge, N.-H.; Jordan, R. E.; Mcneill, J. D.; Harris, C. B. Femtosecond Studies of Electron Tunneling at Metal-Dielectric Interfaces. *Chem. Phys.* **1996**, *205*, 191–203, *Chem. Phys.* **1996**, *208*, 297–298.

(7) Haight, R. Electron Dynamics at Surfaces. *Surf. Sci. Rep.* **1995**, *21*, 277–325.

(8) Harris, C. B.; Ge, N.-H.; Lingle, Jr., R. L.; McNeill, J. D.; Wong, C. M. Femtosecond Dynamics of Electrons on Surfaces and at Interfaces. *Annu. Rev. Phys. Chem.* **1997**, *48*, 711–744.

(9) Richard M. Osgood, J.; Wang, X. Image States on Single-Crystal Metal Surfaces. In *Solid State Physics*; Ehrenreich, H., Spaepen, F., Eds.; Academic Press: New York, Vol. 51, 1998; pp. 1–80.

(10) Petek, H.; Ogawa, S. Femtosecond Time-Resolved Two-Photon Photoemission Studies of Electron Dynamics in Metals. *Prog. Surf. Sci.* **1997**, *56*, 239–310.

(11) Smith, N. V.; Kevan, S. D. Introduction. In *Angle-Resolved Photoemission: Theory*

and Current Applications; Kevan, S. D., Ed.; Elsevier: Amsterdam, 1992; pp. 1–14.

(12) Echenique, P. M.; Pendry, J. B. Theory of Image States at Metal Surfaces. *Prog. Surf. Sci.* **1990**, *32*, 111–172.

(13) Schoenlein, R. W.; Fujimoto, J. G.; Eesley, G. L.; Capehart, T. W. Femtosecond Relaxation Dynamics of Image-Potential States. *Phys. Rev. B* **1991**, *43*, 4688–4698.

(14) Hofer, U.; Shumay, I. L.; Reuss, C.; Thomann, U.; Wallauer, W.; Fauster, T. Time-Resolved Coherent Photoelectron Spectroscopy of Quantized Electronic States on Metal Surfaces. *Science.* **1997**, *277*, 1480–1482.

(15) Firment, L. E.; Somorjai, G. A. Low-Energy Electron Diffraction Study of the Surface of thin Crystals and Monolayers of Normal Paraffins and Cyclohexane on the Ag(111) Crystal Surface. *J. Chem. Phys.* **1978**, *69*, 3940–52.

(16) de Andrés, P. L.; Echenique, P. M.; Flores, F. Lifetime in a Two-Dimensional Image-Potential-Induced Electron Band. *Phys. Rev. B* **1987**, *35*, 4529–32.

(17) Allen, A. O., Drift Mobilities and Conduction Band Energies of Excess Electrons in Dielectric Liquids, NBS Report No. NSRDS-NBS 58, U.S. Dept. of Commerce, 1976.

(18) McNeill, J. D.; Lingle, Jr., R. L.; Ge, N.-H.; Wong, C. M.; Jordan, R. E.; Harris, C. B. Dynamics and Spatial Distribution of Electrons in Quantum Wells at Interfaces Determined by Femtosecond Photoemission Spectroscopy. *Phys. Rev. Lett.* **1997**, *79*, 4645–4648.

(19) Cole, M. Electronic Surface States of a Dielectric Film on a Metal Surface. *Phys. Rev. B* **1971**, *3*, 4418–22.

(20) This calculation is refined from that in Ref.[6] by using the exact WKB expression for the tunneling probability and using the theoretical predicted lifetime scaling[41] for the bare surface lifetime (32, 128, and 384 fs for $n = 1, 2$, and 3, respectively). See Ref.[25] for details.

(21) McNeill, J. D.; Lingle, Jr., R. L.; Jordan, R. E.; Padowitz, D. F.; Harris, C. B. Interfacial Quantum Well States of Xe and Kr Adsorbed on Ag(111). *J. Chem. Phys.* **1996**, *105*, 3883–91.

(22) Lingle, R. L.; Padowitz, D. F.; Jordan, R. E.; Mcneill, J. D.; Harris, C. B. Two-Dimensional Localization of Electrons at Interfaces. *Phys. Rev. Lett.* **1994**, *72*, 2243–2246.

(23) Ge, N.-H.; Wong, C. M.; Lingle, Jr., R. L.; McNeill, J. D.; Gaffney, K. J.; Harris, C. B. Femtosecond Dynamics of Electron Localization at Interfaces. *Science* **1998**, *279*, 202–205.

(24) Wong, C. M.; McNeill, J. D.; Gaffney, K. J.; Ge, N.-H.; Miller, A. D.; Liu, S. H.; Harris, C. B. Femtosecond Studies of Electron Dynamics at Dielectric-Metal Interfaces. *J. Phys. Chem.* **1999**, Jan. 14 in press. In this study the inverse lifetime of the $n = 1$ image state at Xe/Ag(111) interfaces shows a linear dependence on $k_{||}$.

(25) Ge, N.-H. *Ultrafast Studies of Electron Dynamics at Metal-Dielectric Interfaces*, Ph.D. thesis, University of California at Berkeley, 1998.

(26) Interestingly, the decay rate of the $n = 2$ state for a bilayer n-heptane not only decreases with decreasing temperature but also exhibits a linear dependence on $E_{||}$. The mechanism for this $k_{||}^2$ dependence is currently under investigation.

(27) Fischer, R.; Fauster, T.; Steinmann, W. Three-Dimensional Localization of Electrons on Ag Islands. *Phys. Rev. B* **1993**, *48*, 15496–15499.

(28) Landau, L. D. . *Phys. Z. Sowjentunion* **1933**, *3*, 664.

(29) Holstein, T. Studies of Polaron Motion, Part I. The Molecular-Crystal Model. *Ann. Phys.* **1959**, *8*, 325.

(30) Song, K. S.; Williams, R. T. *Self-Trapped Excitons*; Springer-Verlag: Berlin, 1993.

(31) Shluger, A. L.; Stoneham, A. M. Small Polarons in Real Crystals — Concepts and

Problems. *J. Phys.: Condens. Matter* **1993**, *5*, 3049–3086.

(32) Silinsh, E. A.; Čápek, V. *Organic Molecular Crystals : Interaction, Localization, and Transport Phenomen*; American Institute of Physics: New York, 1994.

(33) Emin, D.; Holstein, T. Adiabatic Theory of an Electron in a Deformable Continuum. *Phys. Rev. Lett.* **1976**, *36*, 323–6.

(34) Toyozawa, Y. Electrons, Holes and Excitons in Deformable Lattice. In *Relaxation of Elementary Excitations*; Kubo, R., Hanamura, E., Eds.; Springer-Verlag: Berlin, 1980; pp. 3–18.

(35) Ueta, M.; Kanzaki, H.; Kobayashi, K.; Toyozawa, Y.; Hanamura, E. *Excitonic Processes in Solid*; Springer-Verlag: Berlin, 1986.

(36) Sumi, H. Peculiarities in Exciton-Polaron Formation and Self-Trapping in Low Dimensions. In *Excitonic Processes in Condensed Matter, Proc. SPIE 2362*; Singh, J., Ed.; SPIE: Bellingham, 1995; pp. 108–119.

(37) Marcus, R. A.; Sutin, N. Electron Transfers in Chemistry and Biology. *Biochim. Biophys. Acta* **1985**, *811*, 265.

(38) Ulstrup, J. *Charge Transfer Processes in Condensed Media*; Springer-Verlag: Berlin, 1979.

(39) Stuchebrukhov, A. A.; Song, X. Y. Quantum Effects in Electron Transfer Reactions with Strong Electronic Coupling. *J. Chem. Phys.* **1994**, *101*, 9354–9365.

(40) Snyder, R. G. Vibrational Study of the Chain Conformation of the Liquid n-Paraffins and Molten Polyethylene. *J. Chem. Phys.* **1967**, *47*, 1316.

(41) de Andrés, P. L.; Echenique, P. M.; Flores, F. Calculation of the Lifetimes for Intermediate Rydberg States. *Phys. Rev. B* **1989**, *39*, 10356–8.

TABLES

Table 1: Comparison of measured lifetimes with values calculated from dielectric continuum model.[6,20]

Quantum	Bare (fs)	Monolayer (fs)		Bilayer (fs)		Trilayer (fs)	
Number	Data	Data	Prediction	Data	Prediction	Data	Prediction
$n = 1$	32	155	110	1580	1080	17600	13300
$n = 2$	≤ 20	260	230	500	550	1320	2200
$n = 3$	65	700	640	1000	1020		2700

Figure Captions

Fig. 1. (A) Schematic energy diagram for two-photon photoemission (TPPE). (B) Schematic diagram for the photoejection process of angle-resolved TPPE. The dependence of photoelectron kinetic energy on parallel momentum $\hbar k_{||}$ is illustrated for delocalized and localized states. $E_{\rm vac}$, vacuum energy, $E_{\rm F}$, Fermi energy.

Fig. 2. An electron near a surface is bound by an image potential which the electron induces by polarizing the material. The square of the hydrogenic wavefunction is shown for the lowest two image states. The Ag(111) band structure for $k_{||} = 0$ is shown in shading. The lifetimes for $n = 2, 3$ are anomalously short on Ag(111) due to degeneracy with the conduction band.

Fig. 3. TPPE spectra for the image states showing their change in binding energy as a function of n-heptane layer thickness on Ag(111), taken at a pump-probe delay of 160 fs. Numbers indicate number of layers. The $n = 2, 3$ state region is magnified 10 times for the monolayer.

Fig. 4. (A) Dielectric continuum model potential for a bilayer of n-octane. A potential cutoff is imposed at the metal-layer and layer-vacuum interface to avoid the singularity in the potential. The eigenvalues for the $n = 1$ and 2 states are shown in the dashed lines. (B) The electron probability density for the $n = 1$ and 2 states for 2, 4, 6, and 8 layers of n-octane. The vertial lines represent the layer-vacuum boundary.

Fig. 5. Experimental binding energies ($\circ$) of the $n = 1$ states as a function of n-octane coverage, and a comparison to the results of a dielectric continuum model ($\times$).

Fig. 6. (A) Femtosecond angle-resolved spectra taken at 120 K and a pump-probe delay time of 0 fs and (B) 1670 fs.[23] Initially the electron is in the delocalized state ($m^* = 1.2m_{\rm e}$). The electron then becomes localized within a few hundred femtoseconds. The smaller dispersive feature in (A) is the result of small patches of monolayer interspersed with bilayer.

Fig. 7. Ultrafast time-resolved TPPE traces for (A) delocalized and (B) localized state for

bilayer n-heptane on Ag(111) at various angles and 120 K.[23] The extracted rise time and decay time for the delocalized state at 6° and 20° as well as the corresponding $k_{||}$ are depicted in (A). The spikes near time-zero in (B) for data at high angles come from short-lived electrons on small patches of monolayer.

Fig. 8. Configuration coordinate diagram for self-trapping of an electron. Curves $V_f(k_{||}, Q)$ and $V_s(Q)$ are associated, respectively, with the delocalized states and the self-trapped state. Q is the lattice distortion coordinate. Each curve in the V_f manifold represents a different $k_{||}$ state with a band energy $E_{||}$ ($E_{||} = 0$ at $k_{||} = 0$). The width of the band ($2B$), lattice relaxation energy (E_{rel}), self-trapping energy (E_{st}) and the activation energy of self-trapping (E_a) for $k_{||} = 0$ are depicted. Red arrows indicate the classical barrier crossing from the delocalized to the localized state. Schematic illustration of the electron wavefunction at the n-heptane/Ag(111) interface is shown at the bottom. Left: a delocalized state with $k_{||} = 0.22$ Å^{-1}. Right: a localized state which is assumed to be a 2–D wave packet composed of all $k_{||}$ in the first surface Brillouin zone of the n-heptane lattice.

Fig. 9. (A) Logarithmic plot of self-trapping rate of the delocalized state versus exothermicity for a bilayer at 120 K. The 95% confidence limit for each data point is indicated by the vertical line. The solid line was computed by quantum electron transfer theory[39] with the parameters listed in the figure. (B) Temperature dependence of self-trapping rates for a bilayer at 18° ($k_{||} = 0.21$ Å^{-1}). The solid line was computed with $-\Delta\mathcal{E} = 0.14$ eV and the same parameters as in (A).

Biographical Information

Nien-Hui Ge was born in Taipei, Taiwan, in 1968. She received her B.S. degree from National Taiwan University in 1990, her M.S. degree from National Taiwan University in 1992 under the direction of Lian-Pin Hwang, and her Ph.D. from the University of California at Berkeley in 1998 under the direction of Charles B. Harris. She is currently a postdoctoral fellow at the University of Pennsylvania under the direction of Robin Hochstrasser.

Chung M. Wong was born in Hong Kong in 1971. He received his B.S. degree from Brandeis University in 1994 under the direction of Iu-Yam Chan. He is currently a Ph.D. student at the University of California at Berkeley under the direction of Charles B. Harris.

Charles B. Harris was born in New York, NY, in 1940. He received his B.S. degree from the University of Michigan in 1963 and his Ph.D. from M.I.T. in 1966, under the direction of F.A. Cotton. Following a postdoctoral fellowship in physics from the Atmic Energy Commission at M.I.T., he joined the faculty at the University of California, Berkeley in 1967. He currently holds appointments as Professor of Chemistry at U.C. Berkeley and Principle Investigator, Chemical Sciences Division, Lawrence Berkeley National Laboratory. In addition to his work with ultrafast electronic phenomena at surfaces and at interfaces, his research also focuses on organometallic reaction dynamics.

Word count: 6278 words

Figure 1
Ge et. al.

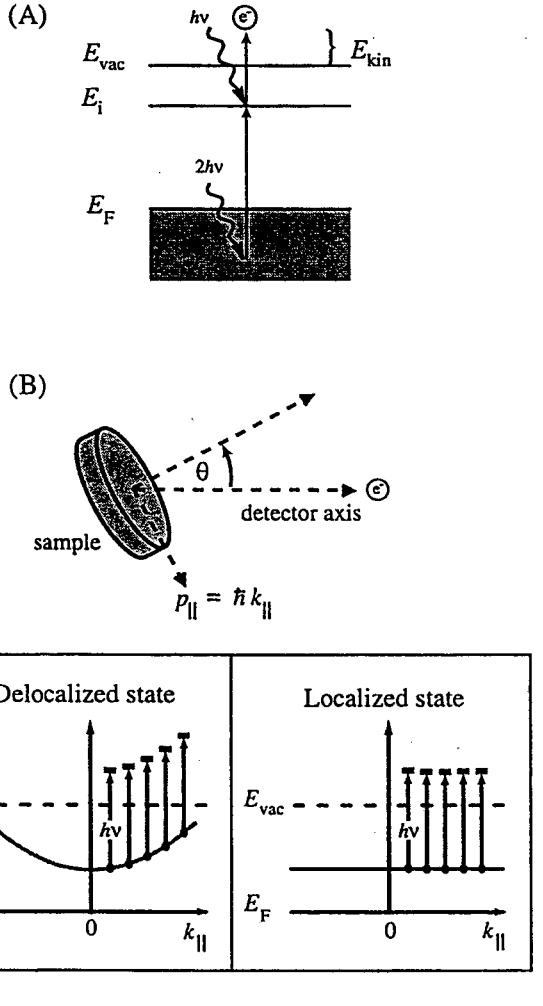

Figure 2
Ge et. al.

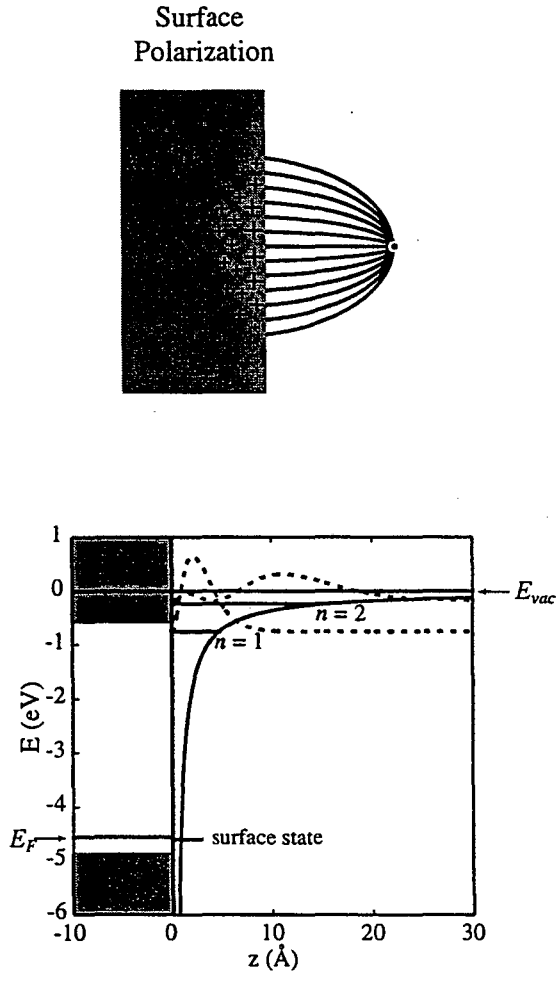

Figure 3
Ge et. al.

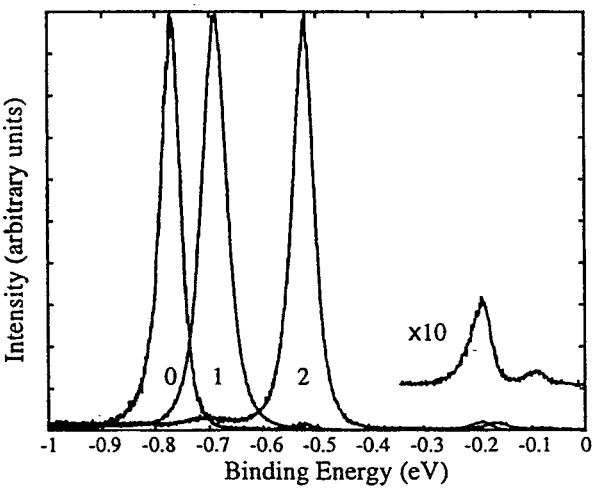

Figure 4
Ge et. al.

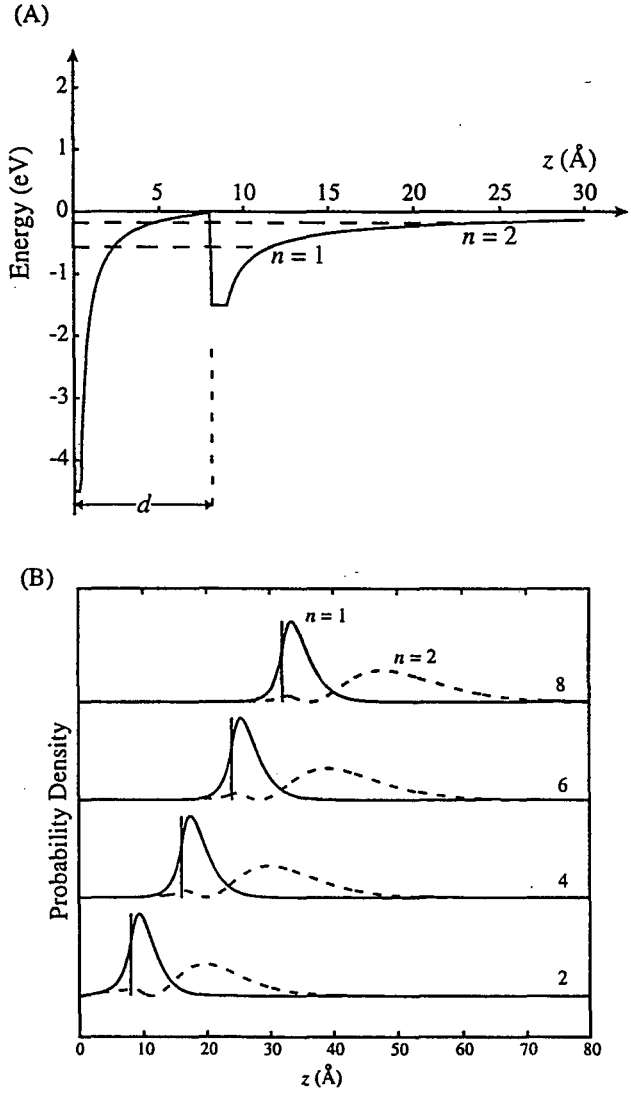

Figure 5
Ge et. al.

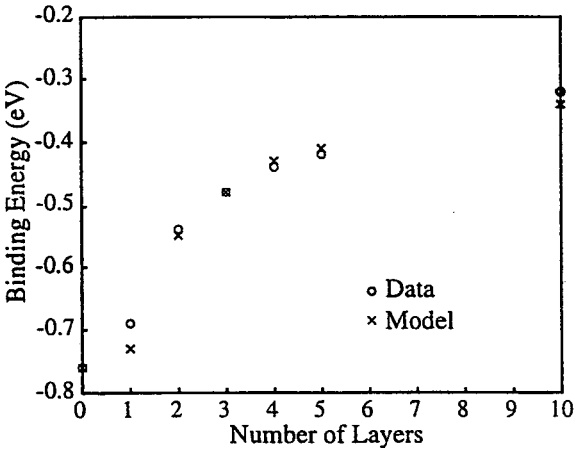

Figure 6
Ge et. al.

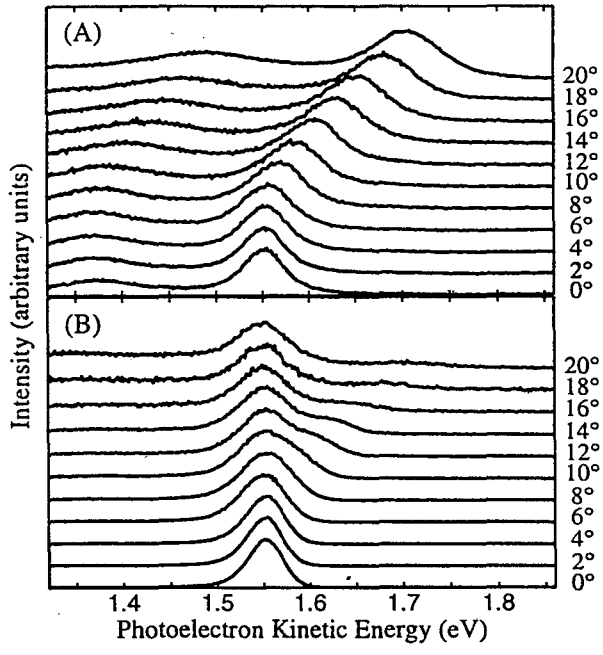

Figure 7
Ge et. al.

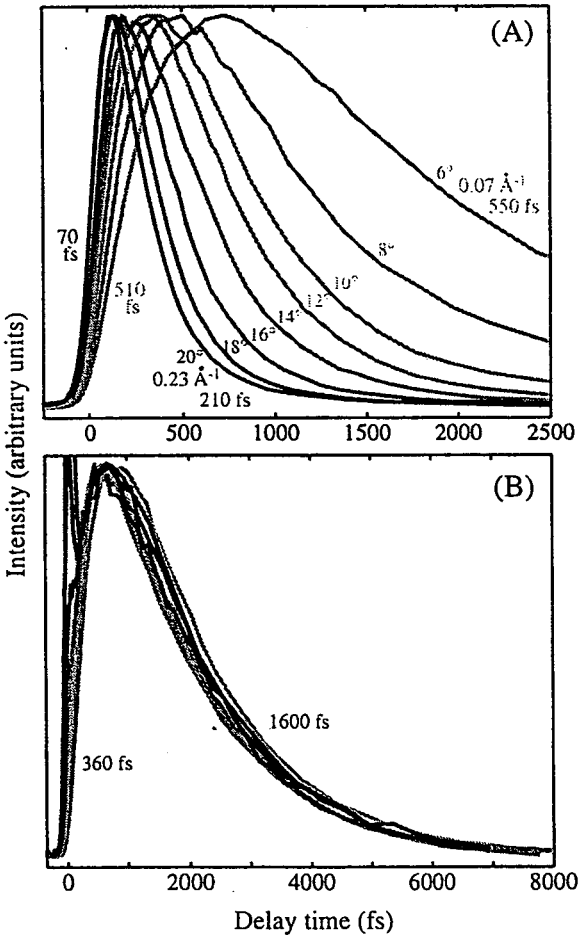

Figure 8
Ge et. al.

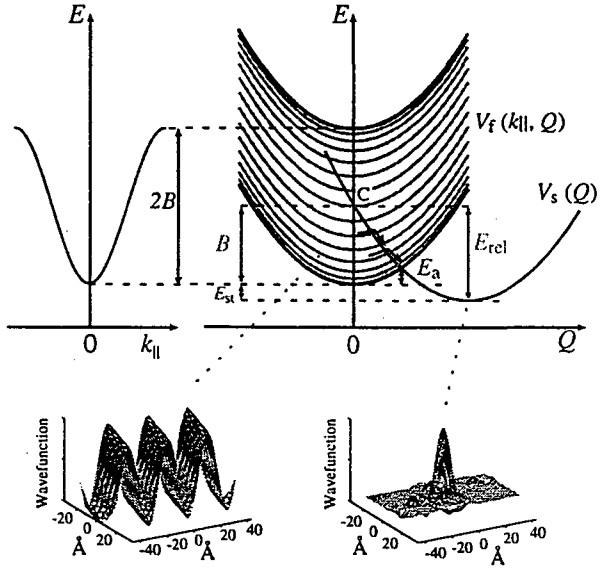

Figure 9
Ge et. al.

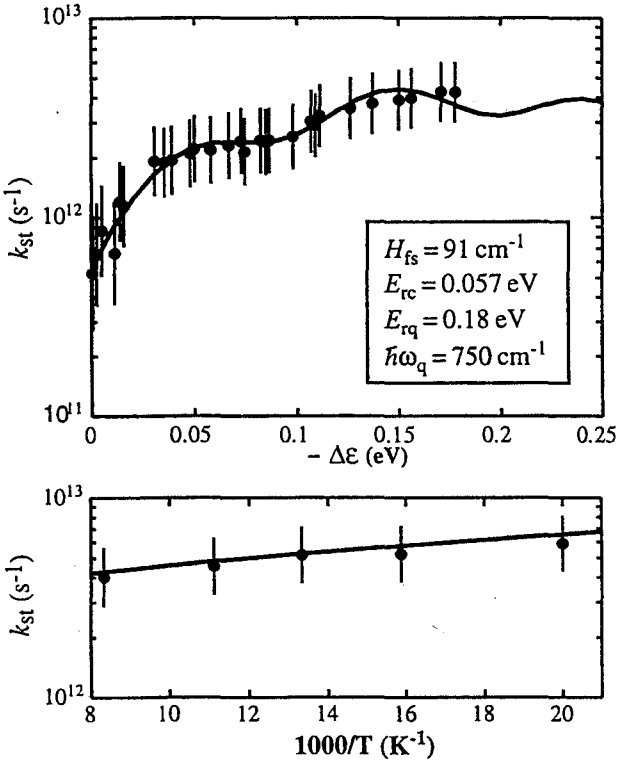

ERNEST ORLANDO LAWRENCE BERKELEY NATIONAL LABORATORY
ONE CYCLOTRON ROAD | BERKELEY, CALIFORNIA 94720

Prepared for the U.S. Department of Energy under Contract No. DE-AC03-76SF00098